Rock Magnetic, Petrography, and Geochemistry Studies of Lava at the Ijen Volcanic Complex (IVC), Banyuwangi, East Java, Indonesia

Aditya Pratama [1,*] **, Satria Bijaksana** [1] **, Mirzam Abdurrachman** [2] **and Nono Agus Santoso** [1]

[1] Faculty of Mining and Petroleum Engineering, Institut Teknologi Bandung, Bandung 40132, Indonesia; satria@fi.itb.ac.id (S.B.), nonoagussantoso2@gmail.com (N.A.S.)

[2] Faculty of Earth Sciences and Technology, Institut Teknologi Bandung, Bandung 40132, Indonesia; mirzam@gc.itb.ac.id

* Correspondence: pratama.itb@gmail.com; Tel.: +62-853-1065-3011

check for updates

Abstract: Lava has complex geochemical characteristics based on differences in eruption centers, eruptive events, and flow emplacement. Characterization of lava is useful for understanding the geological conditions of a volcanic region. To complement geochemical methods, rock magnetic methods are being used to analyze lava. To explore the potential uses of rock magnetic methods for lava characterization, a series of magnetic measurements were completed in lava samples from eight locations in the Ijen Volcanic Complex (IVC) in Banyuwangi, East Java, Indonesia. These locations were grouped into two eruption centers: Ijen Crater and Mount Anyar. The magnetic measurements included frequency-dependent magnetic susceptibility, thermomagnetic, anhysteretic remanent magnetization (ARM), isothermal remanent magnetization (IRM), and hysteresis curve analyses. These measurements were supplemented using X-ray fluorescence, petrography analyses, and Scanning Electron Microscopy with Energy Dispersive Spectroscopy (SEM-EDS). Based on their lithology, lava samples were categorized into basalt, basaltic andesite, and basaltic trachyandesite. The dominant magnetic mineral contained in the sample was iron-rich titanomagnetite and titanium-rich titanomagnetite with a magnetic pseudo-single-domain and small amounts of superparamagnetic grain minerals in some samples. The significant difference in mass specific susceptibility (χ_{LF}) is caused by differences in the crystallization process. The differences in susceptibility frequency dependence (χ_{FD}) highlighted the differences in the magma cooling rate, demonstrated by the differences in the percentage of opaque mineral groundmass. The rock magnetic method was proven to support the geochemistry and petrography methods used to characterize lava and identify the causes of differences in lava characteristics.

Keywords: geochemistry; rock magnetic; lava; volcanic area; Ijen

1. Introduction

Lava has complex characteristics, both vertically and laterally, based on differences in the eruption center, distance of lava outcrop from the eruption center, eruptive events, or the crystallization processes. Due to the complexity of these factors, researchers have extensively studied lava characterization [1–6]. Identification of lava characteristics is useful for understanding the geological conditions of a volcanic region, including the magmatism process and geological history.

Lava characterization is usually conducted by analyzing geochemistry data and petrography [7–12]. However, these methods cannot be used to accurately characterize lava in all cases, such as for the

anisotropy identification of lava flow [13]. Since the 1960s, lava characterization has mainly been conducted using the rock magnetic method, although it was still limited to determining rock structure direction, paleointensity studies, and magnetic evolution of the flow [14–20]. Only a few studies have characterized lava by combining rock magnetic, geochemistry, and petrography methods [21,22]. This combination can provide comprehensive results, including explaining the causes of differences in lava characteristics, which is difficult to obtain if only using the methods in isolation.

This research was conducted at Ijen Crater and Mount Anyar, which are the eruption centers at the Ijen Volcanic Complex (IVC). IVC is a volcanic complex in Indonesia with interesting geological conditions. IVC has many lava units that are well exposed on the surface, especially lava from Ijen Crater and Mount Anyar [23,24]. Distribution of the lava from Ijen Crater and Mount Anyar stretches more than six kilometers from the eruption center (Figure 1), causing the lava to have variations in its characteristics. The studies that have been conducted in IVC were generally related to the lake in the Ijen Crater and its magmatism [25–28], whereas combining the methods to research lava characterization has never been performed.

This research aimed to understand the rock magnetic, geochemistry, and mineralogy characteristics of the lava at Ijen Crater and Mount Anyar. In addition, we explored the role of rock magnetism in explaining the causes of differences in the characteristics of lava.

2. Geological Setting

The IVC is located in the Banyuwangi District, East Java, Indonesia (Figure 1). The IVC is divided into 70 rock units and more than 15 eruption centers [24,29]. The eruption centers located inside the caldera have an area of about 210 km^2 [29]. Each eruption center has a variety of volcanic products, such as lava, pyroclastic flow, and pyroclastic fall.
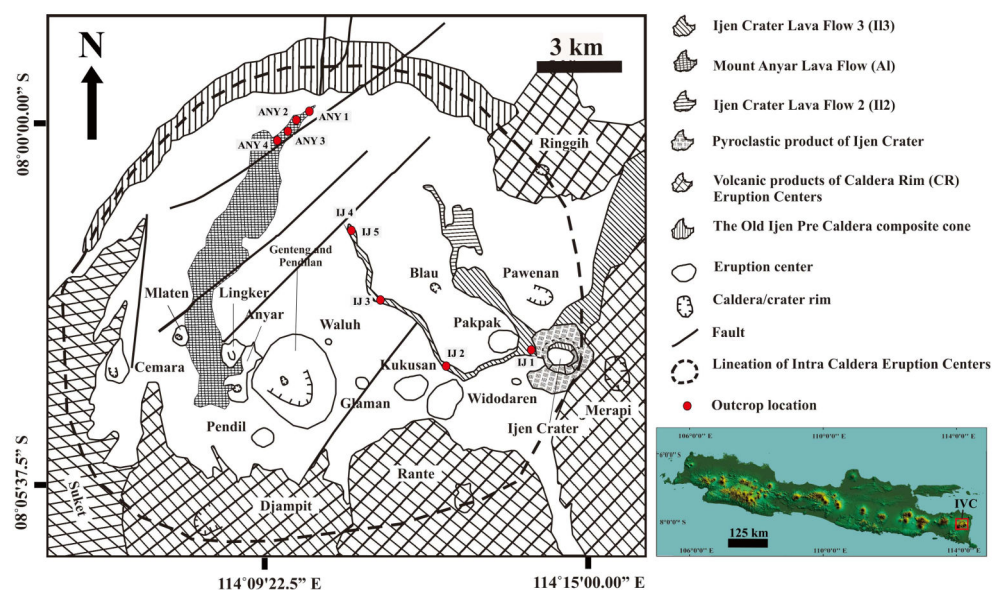
Figure 1. The Ijen Volcanic Complex (IVC) map shows the geographical layout of the eruption centers and the distribution of the volcanic products of some eruption centers [24,27]. Red dots show lava outcrops. Shuttle Radar Topography Mission (SRTM) satellite images were obtained from Earth Data [30].

The Mount Ijen Tua volcanic activity produced big caldera and post caldera volcanic centers. The processes have been described by Caudron et al. [29]. Post caldera volcanic centers can be divided into two groups: Intra Caldera (IC) and Caldera Rim (CR) [27]. Ijen Crater and Mount Anyar are both included in the IC group (Figure 1). Ijen Crater and Mount Anyar have two lava products that are

about 2590 years old, making them the youngest lava in IVC: Ijen Crater Lava Flow 3 (Il3) and Mount Anyar Lava Flow (Al) Formation [24]. Il3 consists of a basalt lithology, whereas Al is a basaltic andesite. In addition, Ijen Crater has older lava products: Lava Crater Ijen 1 (Il3) (~24,000 years ago) and Lava Crater Ijen 2 (Il2) (~9140 years ago) [24]. Lava distribution is shown in Figure 1.

3. Materials and Methods

The study was conducted using nine lava samples directly obtained from Ijen Crater and Mount Anyar. Nine samples were obtained from eight different outcrops spread over two eruption centers: Ijen Crater and Mount Anyar (Figure 1). Five samples (IJ 1, IJ 2, IJ 3, IJ 4, and IJ 5) were products of Ijen Crater and were found along the Banyupahit River. Four other samples (ANY 1, ANY 2, ANY 3, and ANY 4) were obtained from Mount Anyar. IJ 4 and IJ 5 samples were obtained from the same outcrop, but from different lava layers. Eight outcrops were located in different locations and have different lateral distances from the eruption center. Differences in distance from the eruption center can lead to differences in lava characteristics.

Lava samples obtained from these locations were prepared for susceptibility and thermomagnetic measurements, hysteresis parameters, anhysteretic remanent magnetization (ARM), isothermal remanent magnetization (IRM), petrography, and geochemistry. A representative portion of each sample was cut to a thickness of 0.03 mm, and the thin section was analyzed with a Ci-POL polarizing microscope (Nikon, Tokyo, Japan) at the Petrographic Laboratory, Geological Engineering Program, Institut Teknologi Bandung. Identification of magnetic minerals was conducted using back scattered electron (BSE) images of gold-coated, polished thin sections, acquired with JEOL JSM IT300 Scanning Electron Microscopy (SEM) and EX-37270VUP Energy Dispersive Spectroscopy (EDS) by JEOL Ltd., Tokyo, Japan, using an accelerating voltage of 15 kV and probe current of 7.475 nA. This analysis was conducted at the SEM-EDS UPP Chevron Laboratory, Geological Engineering Program, Institut Teknologi Bandung.

A total of 10 g in each sample was crushed to a size of $\leq$50 μm and geochemistry measurements were performed using the Titan Handheld X-ray fluorescence (XRF) S1 by Bruker (Berlin, Germany), at the Petrology Laboratory, Geological Engineering Program, Institut Teknologi Bandung. The precision of this instrument is $\pm$0.5%. Geochemistry element data used in this research included silicon dioxide (SiO_2), aluminium oxide (Al_2O_3), magnesium oxide (MgO), potassium oxide (K_2O), iron (III) oxide (Fe_2O_3), phosphorus pentoxide (P_2O_5), titanium dioxide (TiO_2), and manganese (II) oxide (MnO). The sodium oxide (Na_2O) and Lost of Ignition (LOI) measurements were conducted at the Center Laboratory of Mineral Resources of Coal and Geothermal, Bandung, Indonesia. The sample heating during the LOI measurement was performed using a furnace, whereas Na_2O measurements were performed using the flame photometer method.

For susceptibility, ARM, and IRM measurements, each sample was divided into three parts that were cube-shaped with volume of 1 cm^3. Each cube-shaped sample was inserted into a cylindrical plastic holder with a diameter of 25.4 mm, a height of 22 mm, and a volume of 10 cm^3. All measurements were performed using the tools and steps previously described [31]. The parameters obtained from susceptibility measurements were χ_{LF}, χ_{HF}, and χ_{FD} [31]. ARM measurements produced ARM decay curves that show the Median Destructive Field (MDF) value. This value helps determine the size of a magnetic mineral grain and the type of magnetic domain. In IRM measurements, the magnetic field depends on the electric current. In this study, the magnetic field ranged from 0 to 700 mT. IRM measurements produced IRM saturation curves that show magnetic fields when the curve is saturated, as a basis for determining magnetic minerals contained in rocks. Susceptibility, ARM, and IRM measurements were conducted in the Characterization and Modeling Laboratory of Physical Properties of Rock, Geophysical Engineering Study Program, Institut Teknologi Bandung.

Parts of each sample were crushed to measure the hysteresis parameters using a vibrating sample magnetometer (VSM) as described in previous research [32]. VSM measurement produced hysteresis parameters (M_s, M_{rs}, H_c, and H_{cr}) [32]. In addition, this sample was used for thermomagnetic

measurements using the NMB-89 Magnetic Balance tool from Natsuhara Giken, Osaka, Japan at the Rock Magnetic Laboratory, Marine Advanced Core Research Center, Kochi University, Kochi, Japan.

4. Results and Discussion

Table 1 shows the geochemistry data of XRF measurements of all samples. The samples used were fresh samples, indicated by LOI values of 0.08–2.56 wt % (Table 1). Non-weathered fresh basalt has an LOI value of less than 2.64 wt % [33]. The data in Table 1 was plotted in the total alkali silica (TAS) diagram, which was the table comparing Na_2O, K_2O, and SiO_2 content (Figure 2a) [34]. In addition, geochemistry data [27] were plotted as a comparison.

Table 1. Major elements (% weight) of all samples.

| Sample	IJ 1	IJ 2	IJ 3	IJ 4	IJ 5	ANY 1	ANY 2	ANY 3	ANY 4
MgO	2.54	2.21	2.23	2.56	1.84	3.54	1.79	2.46	2.59
Al_2O_3	22.4	20.3	21.9	19.6	21.9	21.2	23.2	20.7	20.7
SiO_2	51.2	57.0	49.1	56.9	50.4	50.8	51.2	53.8	55.0
P_2O_5	0.25	0.19	0.23	0.19	0.22	0.24	0.20	0.20	0.21
K_2O	0.96	1.67	1.02	1.76	1.05	1.32	0.96	2.31	2.65
CaO	8.22	6.07	8.22	6.30	8.30	8.22	8.59	6.44	6.30
TiO_2	1.12	0.68	0.99	0.90	1.03	1.26	0.94	1.03	1.03
MnO	0.15	0.10	0.13	0.12	0.13	0.15	0.12	0.14	0.14
Fe_2O_3	9.81	7.80	10.5	7.85	10.1	9.84	7.02	7.67	7.86
Na_2O	3.10	2.10	2.65	3.15	2.85	3.30	2.95	3.51	3.97
LOI	0.80	2.28	0.52	1.20	0.92	0.24	2.56	2.40	0.08
Total	101	100	97.5	101	98.7	100	99.5	101	101
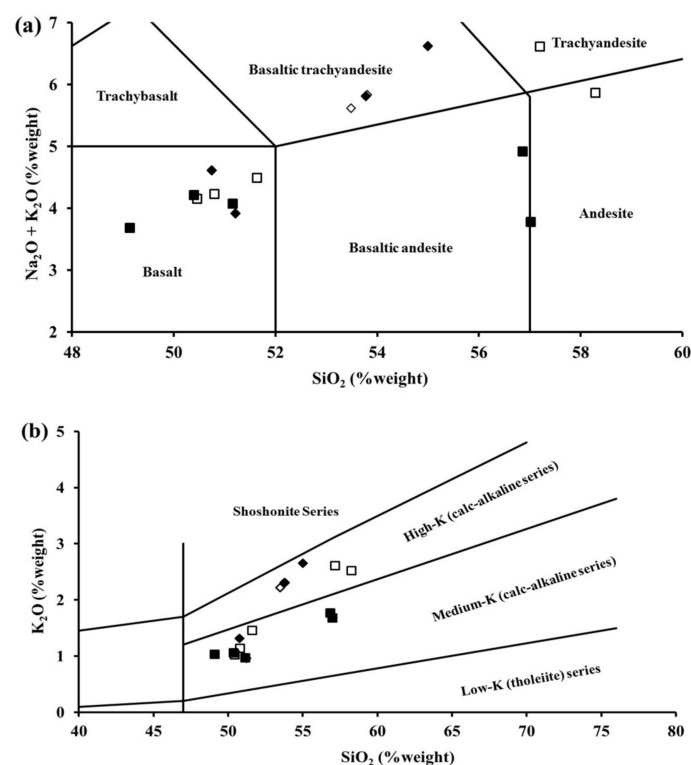
Figure 2. (**a**) Silica oxide (SiO_2) plot versus sodium oxide (Na_2O) and potassium oxide (K_2O) [34]; (**b**) Plot of SiO_2 versus K_2O [35,36]. Symbols: filled square—Ijen Crater (Il3), filled diamond—Mount Anyar (Al), hollow square—Ijen Crater [27], and hollow diamond—Ijen Crater [27].

The TAS diagram classifies volcanic rock based on geochemistry data [35]. Based on Figure 2a, the samples could be classified into three lithologies: basalt, basaltic andesite, and basaltic trachyandesite. Data obtained from a previous study [27] showed that samples from Ijen Crater and Mount Anyar had basalt, andesite, trachyandesite, and basalt trachyandesite lithologies. This difference may arise because the samples used by Handley et al. [27] were obtained from different rock formations than the samples used in this study.

The TAS diagram can also be used to find the magma series [34,36,37] (Figure 2b). Based on Figure 2b, the magma characteristics in the study area are associated with an affinity series of moderate-K calc-alkaline to high-K calc-alkaline. Besides that, basalts from the study area have a titanium oxide (TiO_2) content less than 1.4, indicating volcanic rock that derived from a subduction system [38]. Handley et al. [27] obtained the same results.

Based on petrographic observations, the generally mineralogy of all samples is nearly identical. The phenocryst and microphenocryst predominantly contained in samples included plagioclase, pyroxene, and opaque mineral among the groundmass, which is composed of microlite plagioclase, pyroxene, opaque mineral, and glass. In addition, all samples have a vesicular cavity (porosity) that is characteristic of lava [27]. IJ 1, IJ 3, IJ 5, ANY 1, ANY 2, ANY 3, and ANY 4 had higher microlite abundances compared to IJ 2 and IJ 4 (Figure 3). The detailed petrographic descriptions are explained in the (Supplementary Material Figures S1–S3).
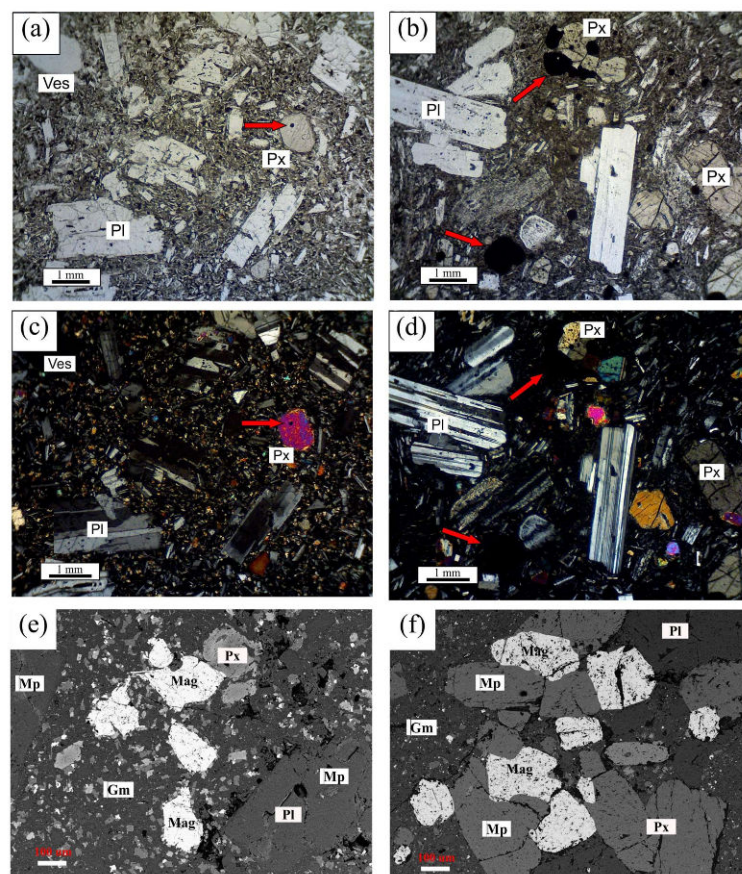

Figure 3. Thin sections show the opaque minerals (red arrow) and the differences of texture in parallel nicol mode of (**a**) IJ 3; (**b**) IJ 4 and cross nicol mode of (**c**) IJ 3; (**d**) IJ 4. BSE images of (**e**) IJ 3 and (**f**) IJ 4, show microphenocryst and groundmass microlite crystal population. Mineral abbreviations: Pl = plagioclase; Px = pyroxene, Ves = vesicular, Mag = titanomagnetite, Gm = groundmass microlite, Mp = microphenocryst.

In the thin section analysis, the magnetic minerals were observed as opaque minerals [39], which were marked by a black color, both cross nicol and parallel nicol modes (Figure 3). Opaque minerals were found as primary minerals in all samples of phenocryst, microphenocryst, and groundmass microlites. Phenocryst is bigger than 0.5, whereas microphenocryst is between 0.125 and 0.5 mm, and groundmass is smaller than 0.125 mm. In general, opaque minerals predominantly present as microlites and often as inclusions within plagioclase and pyroxene minerals in all samples (Figure 3). Some opaque minerals also present as a single mineral among the groundmass. IJ 2 and IJ 4 samples had a larger opaque mineral size compared to other samples (Figure 3). Opaque minerals were mostly found in IJ2, IJ4, and ANY 1 samples (Table S1).

Based on SEM-EDS analysis, the types of magnetic mineral in our samples are Fe-rich titanomagnetite and Ti-rich titanomagnetite (Figure 3). Titanomagnetite crystals are subhedral-anhedral shaped. Samples IJ 3, IJ 5, and ANY 3 have predominantly Ti-rich titanomagnetite, ranging in Ti content from 9.14 to 14.73 mass%. Some Fe-rich titanomagnetite is also found in these samples. Meanwhile, sample IJ 4 has Fe-rich titanomagnetite, with Ti content that is between 6.21 and 7.80 mass%. BSE Images (Figure 3) show that the microlites population of pyroxene, plagioclase, and titanomagnetite of IJ 3 is bigger than IJ 4. The detailed SEM-EDS analysis is explained in the (Supplementary Material Figure S4 and Table S2.

Table 2 shows the rock magnetic data for all samples. The mean values of χ_{LF} and χ_{HF} were 1471.53×10^{-8} m^3/kg and 1451.56×10^{-8} m^3/kg, respectively. In all samples, the mean value of χ_{FD} was 1.47%. In general, the value of χ_{FD} of all samples was less than 2%, indicating that the sample does not contain superparamagnetic grains (SP) [40]. The values of χ_{FD} between 2 and 10%, as in IJ 5, ANY 1, and ANY 4 samples, show that a mixture of SP and non-SP magnetic minerals was present, with a more dominant non-SP grain composition [40]. Figure 4a shows the IRM saturation curves of IJ 2 and ANY 2. These saturation curves were saturated in a field of 150 and 340 mT. The saturation curves of the other samples were saturated in a field of 140–400 mT (Table 2). These results indicate that the magnetic minerals contained in the sample were predominately Fe-rich titanomagnetite and Ti-rich titanomagnetite series [32,41,42].

Figure 5 shows the thermomagnetic curve of some samples. Determination of Curie temperature (*Tc*) through a thermomagnetic curve was previously explained [43]. Thermomagnetic curves of IJ 3, IJ 5, and ANY 3 show multiple *Tc*. These results show that the samples have two phases of magnetic minerals. The presence of magnetite mineral (Fe-rich titanomagnetite) in the samples is supported by the high *Tc* (472–544 °C), whereas the presence of Ti-rich titanomagnetite is supported by the low *Tc* (<400 °C) [41]. This result can be caused by the temperature variation [31].
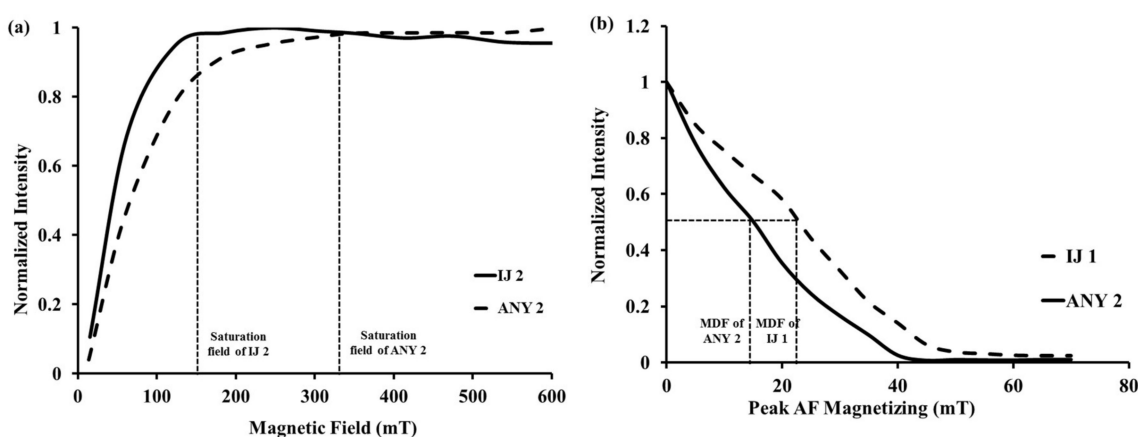
Figure 4. (**a**) Isothermal remnant magnetization (IRM) saturation curve and (**b**) anhysteretic remnant magnetization (ARM) decay curve of some samples. SD: Single Domain, PSD: Pseudo Single Domain, MD: Multi Domain, SP: Superparamagnetic, and MDF: Median Destructive Field.
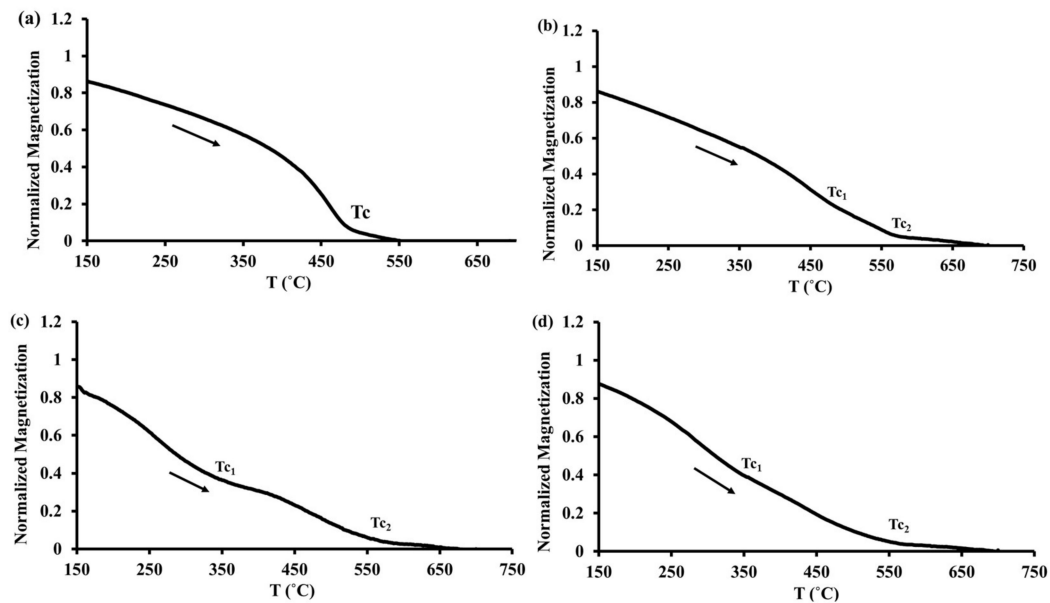
Figure 5. The thermomagnetic curve of (**a**) IJ 2; (**b**) IJ 3; (**c**) IJ 5; and (**d**) ANY 3. *Tc*: Curie Temperature.

Table 2. Rock magnetic data of all samples.

Sample	χ_{LF} ($\times 10^{-8}$ m³/kg)	χ_{HF} ($\times 10^{-8}$ m³/kg)	χ_{FD} (%)	Saturation Field IRM (mT)	Grain Size (µm)	M_{rs}/M_s	H_{cr}/H_c
IJ 1	955.000	949.850	0.54	250	1.00	0.39	1.56
IJ 2	1735.35	1717.10	1.20	150	14.0	0.24	2.29
IJ 3	899.570	882.300	1.92	400	1.50	0.34	1.89
IJ 4	1795.17	1774.13	1.06	140	20.0	0.20	2.81
IJ 5	734.870	720.070	2.02	340	0.60	0.32	1.85
ANY 1	1669.63	1623.27	2.76	240	1.00	0.31	1.78
ANY 2	884.530	865.970	1.58	340	5.00	-	-
ANY 3	1085.00	1073.13	1.39	350	6.00	0.30	1.21
ANY 4	945.830	921.300	2.59	337	6.00	0.26	1.98

Figure 4b shows the ARM decay curve of IJ 1 and ANY 2. Determination of grain size and magnetic domain in rocks with dominant magnetite content can be determined through the identification of MDF on the ARM decay curve [44]. Figure 4b shows that the MDF values of IJ 1 and ANY 2 were 23 and 15 mT, respectively, corresponding to grain sizes of 1 and 5 µm, respectively, for these samples, representing the pseudo-single domain (PSD) [44]. The magnetic domain of all samples was a PSD with a grain size of 0.6–14 µm (Table 2).

These results correspond to the hysteresis parameter analysis. Table 2 also compares the magnetic hysteresis parameters (M_{rs}/M_s and H_c/H_c) in all samples. The value was then plotted on the Day's Plot curve to find the type of magnetic domain (Figure 6) [45], and to confirm the results obtained through the ARM measurements. In general, the entire magnetic domain of the samples was included in the PSD (Figure 6).

The petrographic observation results correspond to the rock magnetic analysis. The magnetic susceptibility value (χ_{LF}) was proportional to the percentage of opaque minerals (Figure 7). Figure 7 shows that one of the factors affecting the χ_{LF} value is the quantity of magnetic minerals. The nine samples from Ijen Crater and Mount Anyar could be divided into two groups: Group 1 (IJ 1, IJ 3, IJ 5, ANY 2, ANY 3, and ANY 4) had a χ_{LF} value of 734.87–1085 $\times 10^{-8}$ m³/kg, whereas the χ_{LF} value of group 2 (IJ 2, IJ 4, and ANY 1) was 1669.63–1795.17 $\times 10^{-8}$ m³/kg. In addition, the percentages of microlites of both groups were different. Group 1 has a greater percentage of microlites, at 44–50%, than Group 2, at 33–46% (Table S1).
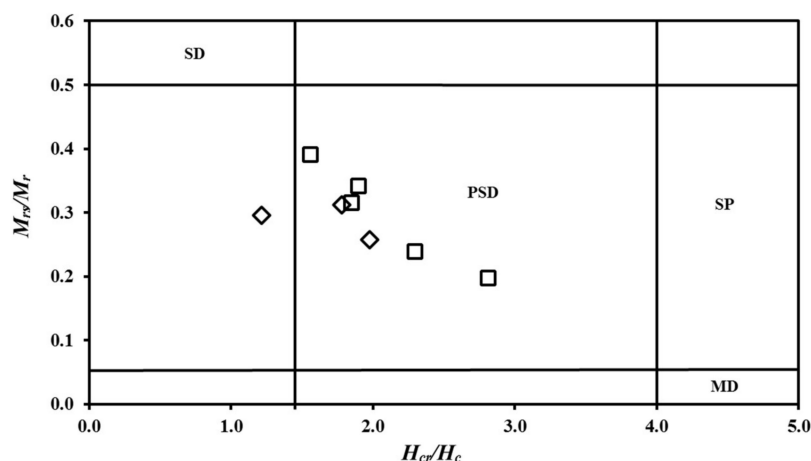
Figure 6. Hysteresis parameters on a Day's Plot [45] for all samples. SD: Single Domain, PSD: Pseudo Single Domain, MD: Multi Domain, SP: Superparamagnetic. Symbols: hollow square—Ijen Crater, hollow diamond—Mount Anyar.

In addition to the quantity of magnetic minerals, the difference in magnetic mineral phase causes differences in the susceptibility of both groups. Magnetic minerals in Group 1 were predominantly Ti-rich titanomagnetite with a *Tc* value of approximately 350 °C, and little Fe-rich titanomagnetite with a *Tc* of 536–544 °C. The predominant magnetic mineral in Group 2 was Fe-rich titanomagnetite with a *Tc* of approximately 472 °C. The magnetic mineral phase difference in both groups was also supported by the differences in the IRM saturation curve pattern (Figure 4a) and the SEM-EDS analysis. In general, the IRM saturation field in Group 1 was higher than 300 mT, whereas that in Group 2 was lower than 300 mT (Table 2).
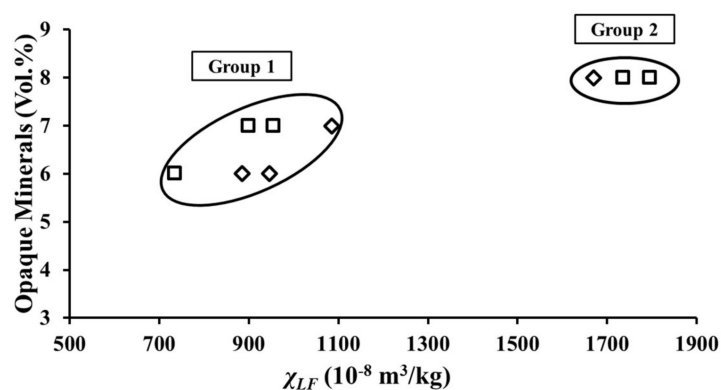
Figure 7. Plot between the percentage of opaque minerals with low frequency susceptibility in samples from Ijen Crater (hollow square) and Mount Anyar (hollow diamond) (modified from Pratama et al. [39]).

The crystallization process in an eruptive event can be different. For example, in a 2006 eruption, Preece et al. [46] recorded a variety of microlites' abundances and shapes in the dome of Merapi Volcano, Indonesia. They interpreted that these variations were caused by differences in the crystallization process, which may occur during ascent and dome residence. The present results suggest that a similar process may have occurred in the Ijen Crater lava flow 3 and Mount Anyar lava flow. In an eruptive event, crystallization occurred under different magma ascent and lava residence conditions. Higher undercooling and magma ascent leads to an increased nucleation rate, producing the abundant microlites in the samples, and vice versa [46,47]. In addition, based on Zhou et al. [47], higher undercooling leads to the formation of two phases of titanomagnetite (Fe-rich and Ti rich

titanomagnetite). Meanwhile, the magnetization of magnetic mineral decreases with an increasing Ti content [48,49]. The presence of Ti-rich titanomagnetite may decrease the susceptibility value. Even, Lauro et al. [50] showed that the weathered volcanic rock/soil on Mount Etna which contains titanoferous-magnetite was not magnetic.

The samples which had a similar χ_{LF} value and microlites abundances (assuming that the samples were produced from the same crystallization process) had different percentages of opaque mineral groundmass and porosity (Table S1). The mineral size in lava determines the magma cooling rate. The faster the magma cooling, the smaller the size of the mineral formed. The percentage of porosity is strongly influenced by stress [51]. Little stress in the lava flow causes the porosity of igneous rock to increase. Cooling rate and stress at a lava layer are associated with a top–bottom position, known as the vertical stratigraphic position. At the top of the lava layer, magma cooling is faster, and the stress is smaller, thus the minerals formed are smaller with a higher porosity percentage, and vice versa.

In addition, the percentage of χ_{FD} in the sample was different and proportional to the percentage of the opaque mineral groundmass and porosity. Figure 8 shows the plot between χ_{FD} with the percentage of groundmass of opaque minerals and the percentage of porosity in some samples, which we estimate to be generated during the same crystallization process. The value of χ_{FD} indicates the presence of SP in a rock sample [40,52]. The high presence of SP grains is related to the fast magma/lava cooling process caused by being relatively near to the surface. Rapid magma cooling can form titanomagnetite-series minerals smaller than 1 μm [49]. This result shows that χ_{FD} can be used to determine the vertical sample location (difference in the cooling rate).
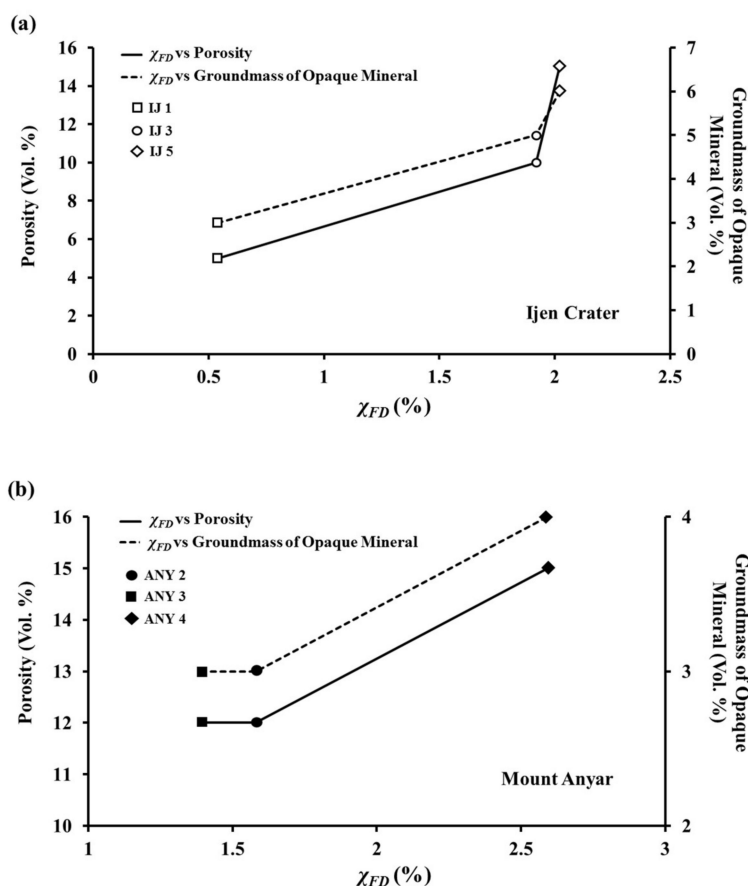

Figure 8. Plots between the percentage of groundmass of opaque mineral and porosity with susceptibility frequency dependence (χ_{FD}) of (**a**) IJ 1, IJ 3, and IJ 5 samples; and (**b**) ANY 2, ANY 3, and ANY 4 samples.

For example, the IJ 1, IJ 3, and IJ 5 samples were likely produced from the same crystallization process, but these samples have different χ_{FD} values, percentages of groundmass of opaque mineral, and porosity (Table S1). The IJ 1 sample had a smaller χ_{FD}, groundmass of opaque mineral, and porosity value than IJ 3 and IJ 5. Conversely, IJ 5 had the greatest value. The results show that IJ 5 was at the top of the layer, whereas IJ 1 was at the bottom. The difference in the vertical position of these samples was also observed from the hand specimen (Figure 9). The IJ 1 porosity was much less than that of IJ 5.
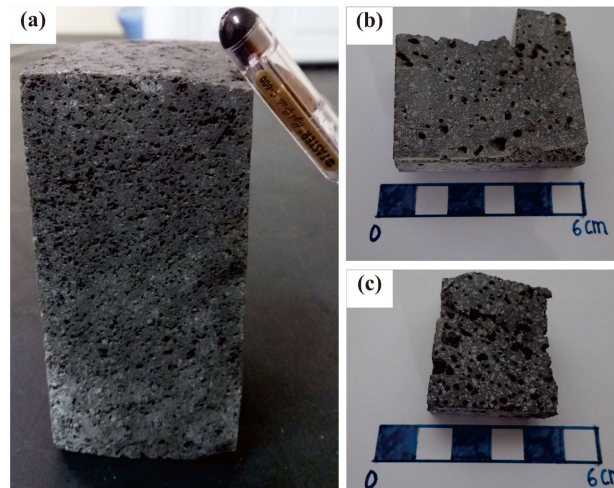
Figure 9. Hand specimen of (**a**) IJ 1; (**b**) IJ 3; and (**c**) IJ 5 samples.

Figure 10 shows a plot between χ_{LF} and χ_{FD} of the lava samples from Ijen Crater and Mount Anyar and igneous rock dyke samples from Co. Fermanagh, Northern Ireland [53]. Figure 10 shows that the lava (extrusive igneous rock) and dyke (intrusive igneous rock) samples have similar rock magnetic characteristics. In addition, based on the value of χ_{LF}, both the lava and dyke samples could be divided into two groups. Samples in the same group had different χ_{FD} values. The difference in the χ_{LF} and χ_{FD} values for the dyke samples Co. Fermanagh, Northern Ireland was caused by the differences in the rock forming time and magma cooling rate [53]. This result corresponds to our results above.
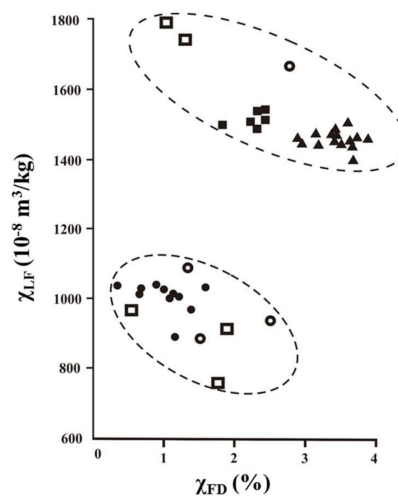
Figure 10. Plot between mass specific susceptibility (χ_{LF}) and χ_{FD} of lava samples from Ijen Crater (hollow square) and Mount Anyar (hollow circle), and dyke samples from Co. Fermanagh, Northern Ireland (site A: filled square, site C: filled triangle, site E: filled circle) [53].

5. Conclusions

Lava from Ijen Crater (Il3) and Mount Anyar (Al) could generally be classified into basalt, basaltic andesite, and basaltic trachyandesite lithology with moderate-K calc-alkaline to high-K calc-alkaline magma series. The magnetic susceptibility of all samples was 734.870–1795.17 $\times$ 10^{-8} m^3/kg. The dominant magnetic mineral contained in the samples was Fe-rich titanomagnetite and Ti-rich titanomagnetite with a PSD magnetic domain. In some samples, we also found small amounts of SP minerals. Based on mass specific susceptibility (χ_{LF}), nine samples could be divided into two groups. They had differences in rock texture, quantity of magnetic mineral, and magnetic mineral phase. The differences in the samples' characteristics from the same eruption center can be caused by a difference in the crystallization process. Additionally, some samples which were produced from the same crystallization process had differences in χ_{FD}, percentage of porosity, and groundmass of opaque mineral. The variation in these variables can be caused by the differences in the magma/lava cooling rate, which shows the vertical stratigraphic position of the samples in a lava layer. So, the analysis of this rock magnetic data supports the available geochemistry data, as well as the petrographic analysis data, when characterizing lava from Ijen Crater and Mount Anyar.

References

1. Carr, M.J. Symmetrical and segmented variation of physical and geochemical characteristics of the Central American volcanic front. *J. Volcanol. Geotherm. Res.* **1984**, *20*, 231–252. [CrossRef]
2. Cañón-Tapia, E.; Walker, G.P.; Herrero-Bervera, E. The internal structure of lava flows—Insights from AMS measurements II: Hawaiian pahoehoe, toothpaste lava and 'a'ā. *J. Volcanol. Geotherm. Res.* **1997**, *76*, 19–46. [CrossRef]
3. Rüpke, L.H.; Morgan, J.P.; Hort, M.; Connolly, J.A. Are the regional variations in Central American arc lavas due to differing basaltic versus peridotitic slab sources of fluids? *Geol. Soc. Am.* **2002**, *30*, 1035–1038. [CrossRef]
4. Schaefer, C.J.; Kattenhorn, S.A. Characterization and evolution of fractures in low-volume pahoehoe lava flows, eastern Snake River Plain, Idaho. *Geol. Soc. Am. Bull.* **2004**, *116*, 322–336. [CrossRef]
5. Single, R.T.; Jerram, D.A. The 3D facies architecture of flood basalt provinces and their internal heterogeneity: Examples from the Paleogene Skye Lava Field. *J. Geol. Soc.* **2004**, *161*, 911–926. [CrossRef]
6. Fukuma, K. Vertical Variation of Testing Thellier Paleointensities from a Recent Lava Flow in Japan. In Proceedings of the 9th International Conference "Problems of Geocosmos", St. Petersburg, Russia, 8–12 October 2012; pp. 29–42.
7. MacDonald, G.A.; Katsura, T. Variations in the lava of the 1959 eruption in Kilauea Iki. *Pac. Sci.* **1961**, *15*, 358–369.
8. Watkins, N.D.; Haggerty, S.E. Primary oxidation variation and petrogenesis in a single lava. *Contrib. Mineral. Petrol.* **1967**, *15*, 251–271. [CrossRef]
9. Rhodes, J.M. Homogeneity of lava flows: Chemical data for historic Mauna Loan eruptions. *J. Geophys. Res. Sol. Earth* **1983**, *88*, A869–A879. [CrossRef]

10. O'Reilly, S.Y.; Zhang, M. Geochemical characteristics of lava-field basalts from eastern Australia and inferred sources: Connections with the subcontinental lithospheric mantle? *Contrib. Mineral. Petrol.* **1995**, *121*, 148–170. [CrossRef]

11. Kocak, K.; Zedef, V. Geochemical characteristics of the lava domes in Yatagan village and Sağlik town, from Erenlerdagi (Konya, Central Turkey) volcanites. *Act. Geobalcanica* **2016**, *2*, 7–19. [CrossRef]

12. Polo, L.A.; Janasi, V.A.; Giordano, D.; Lima, E.F.; Cañon-Tapia, E.; Roverato, M. Effusive silicic volcanism in the Paraná Magmatic Province, South Brazil: Evidence for locally-fed lava flows and domes from detailed field work. *J. Volcanol. Geotherm. Res.* **2017**, in press. [CrossRef]

13. Cañón-Tapia, E.; Coe, R. Rock magnetic evidence of inflation of a flood basalt lava flow. *Bull. Volcanol.* **2002**, *64*, 289–302. [CrossRef]

14. Wilson, R.L.; Haggerty, S.E.; Watkins, N.D. Variation of palaeomagnetic stability and other parameters in a vertical traverse of a single Icelandic lava. *Geophys. J. Int.* **1968**, *16*, 79–96. [CrossRef]

15. Rolph, T.C. An investigation of the magnetic variation within two recent lava flows. *Geotherm. J. Int.* **1997**, *130*, 125–136. [CrossRef]

16. Mena, M.; Orgeira, M.J.; Lagorio, S. Paleomagnetism, rock-magnetism and geochemical aspects of early Cretaceous basalts of the Paraná Magmatic Province, Misiones, Argentina. *Earth Planets Space* **2006**, *58*, 1283–1293. [CrossRef]

17. Dietze, F.; Kontny, A.; Heyde, I.; Vahle, C. Magnetic anomalies and rock magnetism of basalts from Reykjanes (SW-Iceland). *Stud. Geophys. Geod.* **2011**, *55*, 109–130. [CrossRef]

18. Almqvist, B.S.G.; Bosshard, S.A.; Hirt, A.M.; Mattsson, H.B.; Hetényi, G. Internal flow structures in columnar jointed basalt from Hrepphólar, Iceland: II. Magnetic anisotropy and rock magnetic properties. *Bull. Volcanol.* **2012**, *74*, 1667–1681. [CrossRef]

19. Kapper, L.; Morales, J.; Calvo-Rathert, M.; Goguitchaichvili, A.; Mejia, V.; Caccavari, A.; Guevara, A.N.; Ruiz, R.C. A paleointensity study of Cretaceous volcanic rocks from the Western Cordillera, Colombia. *Stud. Geophys. Geod.* **2017**, *61*, 264–289. [CrossRef]

20. Cervantes-Solano, M.; Kapper, L.; Goguitchaichvili, A.; Ruiz-Martínez, V.C.; Rosas-Elguera, J.; Morales, J.; Maciel-Peña, R.; Cejudo-Ruiz, R. A detailed paleomagnetic and rock-magnetic investigation around Cretaceous-Paleogene boundary: The Autlan (Western Mexico) volcanic sequence revisited. *Stud. Geophys. Geod.* **2017**, *61*, 233–248. [CrossRef]

21. McEnroe, S.A.; Brown, L.L. Palaeomagnetism, rock magnetism and geochemistry of Jurassic dykes and correlative redbeds, Massachusetts, USA. *Geotherm. J. Int.* **2000**, *143*, 22–38. [CrossRef]

22. Alva-Valdivia, L.M.; Bohnel, H.; McIntosh, G.; Caballero-Miranda, C.; Morales, J. Vertical Detailed Variation of Petromagnetic Properties in Basalt Flow Profiles, Xitle Volcano, Mexico: A Review. *Latinmag Lett.* **2011**, *1*, D14.

23. Siddiq, F. Volcanostratigraphy and Petrogenesis of Mount Ijen, Banyuwangi District, East Java. Bachelor's Thesis, Institut Teknologi Bandung, Bandung, Indonesia, 2015.

24. Sujanto; Syarifuddin, M.Z.; Sitorus, K. *Geological Map of the Ijen Caldera Complex, East Java*; Volcanology Survey of Indonesia: Bandung, Indonesia, 1988.

25. Delmelle, P.; Bernard, A. Downstream composition changes of acidic volcanic waters discharged into the Banyupahit stream, Ijen caldera, Indonesia. *J. Volcanol. Geotherm. Res.* **2000**, *97*, 55–75. [CrossRef]

26. Delmelle, P.; Bernard, A.; Kusakabe, M.; Fischer, T.P.; Takano, B. Geochemistry of the magmatic–hydrothermal system of Kawah Ijen volcano, East Java, Indonesia. *J. Volcanol. Geotherm. Res.* **2000**, *97*, 31–53. [CrossRef]

27. Handley, H.K.; Macpherson, C.G.; Davidson, J.P.; Berlo, K.; Lowry, D. Constraining Fluid and Sediment Contributions to Subduction-Related Magmatism in Indonesia: Ijen Volcanic Complex. *J. Petrol.* **2007**, *48*, 1155–1183. [CrossRef]

28. Van Hinsberg, V.; Berlo, K.; Sumarti, S.; van Bergen, M.; Williams-Jones, A. Extreme alteration by hyperacidic brines at Kawah Ijen volcano, East Java, Indonesia: II. *J. Volcanol. Geotherm. Res.* **2010**, *196*, 169–184. [CrossRef]

29. Caudron, C.; Syahbana, D.K.; Lecocq, T.; Van Hinsberg, V.; McCausland, W.; Triantafyllou, A.; Camelbeeck, T.; Bernard, A. Surono Kawah Ijen volcanic activity: A review. *Bull. Volcanol.* **2015**, *77*. [CrossRef]

30. Earth Data. Available online: https://earthdata.nasa.gov/ (accessed on 2 November 2017).

31. Santoso, N.A.; Bijaksana, S.; Kodama, K.; Santoso, D.; Dahrin, D. Multimethod Approach to the Study of Recent Volcanic Ashes from Tengger Volcanic Complex, Eastern Java, Indonesia. *Geosciences* **2017**, *7*, 63. [CrossRef]

32. Sudarningsih, S.; Bijaksana, S.; Ramdani, R.; Hafidz, A.; Pratama, A.; Widodo, W.; Iskandar, I.; Dahrin, D.; Fajar, S.J.; Santoso, N.A. Variations in the Concentration of Magnetic Minerals and Heavy Metals in Suspended Sediments from Citarum River and Its Tributaries, West Java, Indonesia. *Geosciences* **2017**, *7*, 66. [CrossRef]

33. Tugrul, A.; Gurpinar, O. The Effect of Chemical Weathering on the Engineering Properties of Eocene Basalts in Northeastern Turkey. *Environ. Eng. Geosci.* **1997**, *3*, 225–234. [CrossRef]

34. Le Bas, M.J.; Le Maitre, R.W.; Streckeisen, A.; Zanettin, B. A chemical classification of volcanic rocks based on the total alkali-silica diagram. *J. Petrol.* **1986**, *27*, 745–750. [CrossRef]

35. LeMaitre, R.W. *Igneous Rocks: A Classification and Glossary of Terms*; Cambridge University Press: Cambridge, UK, 2005; pp. 30–39, ISBN 978-0-521-66215-4.

36. Peccerillo, A.; Taylor, S.R. Geochemistry of Eocene calc-alkaline volcanic rocks from the Kastamonu area, northern Turkey. *Contrib. Mineral. Petrol.* **1976**, *58*, 63–81. [CrossRef]

37. Wilson, M. *Igneous Petrogenesis*; Springer: Dordrecht, The Netherlands, 2007; pp. 1–100, ISBN 978-0-412-53310-5.

38. Metcalf, R.V.; Shervais, J.W. Suprasubduction-zone ophiolites: Is there really an ophiolite conundrum? *Geol. Soc. Am.* **2008**, *438*, 191–222. [CrossRef]

39. Pratama, A.; Hafidz, A.; Bijaksana, S.; Abdurrachman, M. Basaltic lava characterization using magnetic susceptibility identification and presence of opaque minerals in Ijen volcanic complex, Banyuwangi, East Java. *AIP Conf. Proc.* **2017**, *1861*, 030054. [CrossRef]

40. Dearing, J.A. *Environmental Magnetic Susceptibility: Using the Bartington MS2 System*; Chi Pub.: Kenilworth, UK, 1994; pp. 30–50, ISBN 0-9523409-0-9.

41. Liebke, U.; Antolin, B.; Appel, E.; Basavaiah, N.; Mikes, T.; Dunkl, I.; Wemmer, K. Indication for clockwise rotation in the Siang window south of the eastern Himalayan syntaxis and new geochronological constraints for the area. *Geol. Soc. Lond. Spec. Publ.* **2011**, *353*, 71–97. [CrossRef]

42. Chi, C.T.; Dorobek, S.T. Cretaceous paleomagnetism of Indochina and surrounding regions: Cenozoic tectonic implications. *Geol. Soc. Lond. Spec. Publ.* **2004**, *226*, 273–287. [CrossRef]

43. Tauxe, L. *Paleomagnetic Principles and Practice*; Kluwer Academic Publishers: Dordrecht, The Netherlands, 2003; pp. 30–90, ISBN 978-0-306-48128-4.

44. Dunlop, D.J.; Özdemir, Ö. *Rock Magnetic: Fundamentals and Frontiers*; Cambridge studies in magnetism; Cambridge University Press: Cambridge, NY, USA, 1997; pp. 1–120, ISBN 978-0-521-32514-1.

45. Day's, R.; Fuller, M.D.; Schmidt, V.A. Hysteresis properties of titanomagnetites: Grain size and composition dependence. *Phys. Earth Planet. Inter.* **1977**, *13*, 260–266.

46. Preece, K.; Barclay, J.; Gertisser, R.; Herd, R.A. Textural and micro-petological variations in the eruptive products of the 2006 dome-forming eruption of Merapi volcano, Indonesia: Implications for sub-surface processes. *J. Volcanol. Geotherm. Res.* **2013**, *261*, 98–120. [CrossRef]

47. Zhou, W.; Van der Voo, R.; Peacor, D.R.; Zhang, Y. Variable Ti-content and grain size of titanomagnetite as a function of cooling rate in very young MORB. *Earth Planet. Sci. Lett.* **2000**, *179*, 9–20. [CrossRef]

48. Jordanova, N. *Soil Magnetism: Applications in Pedology, Environmental Science and Agriculture*; Academic Press: London, UK, 2017; pp. 2–3.

49. Butler, R.F. *Paleomagnetism: Magnetic Domains to Geologic Terranes*; Blackwell Scientific Publications: Hoboken, NJ, USA, 1998; p. 25.

50. Lauro, S.E.; Mattei, E.; Cosciotti, B.; Di Paolo, F.; Arcone, S.A.; Viccaro, M.; Pettinelli, E. Electromagnetic signal penetration in a planetary soil simulant: Estimated attenuation rates using GPR and TDR in volcanic deposits on Mt. Etna. *J. Geophys. Res. Planet* **2017**, *122*, 1392–1404. [CrossRef]

51. Schaefer, L.N.; Kendrick, J.E.; Oommen, T.; Lavallée, Y.; Chigna, G. Geomechanical rock properties of a basaltic volcano. *Front. Earth Sci.* **2015**, *3*, 1–15. [CrossRef]

52. Sudarningsih, S.; Maulana, L.; Bijaksana, S.; Hafidz, A.; Pratama, A.; Widodo, W.; Iskandar, I. Magnetic Characterization of Sand and Boulder Samples from Citarum River and Their Origin. *J. Math. Fundam. Sci.* **2017**, *49*, 116–126. [CrossRef]

53. Gibson, P.J.; Lyle, P.; Thomas, N. Magnetic Characteristics of the Cuilcagh Dyke, Co. Fermanagh, Northern Ireland. *Irish J. Earth Sci.* **2009**, *27*, 1–9. [CrossRef]